A Noncovalent Interaction Insight onto the Concerted Metallation Deprotonation Mechanism

Yann Cornaton, Jean-Pierre Djukic

A Noncovalent Interaction Insight onto the Concerted Metallation Deprotonation Mechanism.

Received 00th January 20xx,
Accepted 00th January 20xx

DOI: 10.1039/x0xx00000x

Yann Cornaton [a,b] and Jean-Pierre Djukic[b]*

The CMD/AMLA mechanisms of cyclopalladation and the parent fictitious but challenging cyclonickelation of *N,N*-dimethylbenzylamine have been investigated by joint DFT-D and DLPNO-CCSD(T) methods assisted by QTAIM-based nocovalent interaction plots (NCI plots) and interacting quantum atoms (IQA) analyses, and the local energy decomposition (LED) procedure. Bader charges, NCI plots, IQA and the LED analyses clearly suggest that coulombic interactions play an important role and somewhat govern the whole process that is sensitive to the charge borne by the metal centre. It is found that replacement of acetate by acetamidate used as a ligand and a base significantly lowers the barrier to the formation of the key agostic intermediate. The latter shows a peculiar polarization by its immediate ligand environment where a significant electrostatic CH…O interaction with the neighboring carboxylato ligand competes with the strong propensity of the latter to bind the metal center, which is stronger in the agostic intermediate when the carboxylato ligand is the acetate and when the metal is Ni. It is also shown that the hereby idealized cyclonickelation is disfavored as compared to cyclopalladation owing to enhanced electrostatic repulsion in almost all stages of the CMD mechanism.

Introduction

C-H bond activation and functionalization represent challenging goals in modern homogeneous catalysis.[1, 2] The Concerted Metallation Deprotonation (CMD)° mechanism, often assimilated to the Ambiphilic Metal Ligand Activation (AMLA) mechanism[3-5] is a flexible way to achieve carbometallation that has been particularly developed in Pd(II)-based catalysis and is being used extensively nowadays to promote a host of sophisticated functionalizations of organic compounds.[1, 6] If the intimate nature of the agostic C-H…M bond remains a matter of interest and debate, it has long been stressed that it should not be considered strictly as a 3-center/2-electron interaction, neither as a non-covalent interaction.[7, 8] The concept of "syndetic donation" has been put forward by Nielson, Harrison and co-workers[9, 10] to characterize the weak donor-acceptor (charge transfer) "covalent" interactions established between the σ-C-H bonding orbital and Pd vacant *d* orbital with electron density donation from the neighbouring π-system, with variable back donation occurring from the Pd centre to the σ* orbital of the C-H bond in the agostic intermediate.[11] A recent DLPNO-CCSD(T)[12]-based investigation by Neese and co-workers[13] outlined the role played by dispersion[14] in the stabilization of known agostic C-H…metal complexes, thus opening a new perspective for the investigation of key agostic intermediates in the CMD/AMLA mechanism that outranks the orbital-based[15] Dewar[16]-Chatt-Duncanson[17] analysis of bond making/unmaking. [13]

One missing factor in most studies of the CMD mechanism is indeed the role of non-covalent interactions. In a complex molecular system were a C-H bond is engaged in agostic interactions of weak covalent character with a metal centre it is tempting to consider the coordination environment of the metal consisting of auxiliary bases and ligands as a local multipole,[18] which might also contribute to the chemical activation of the C-H bond as external electric fields do.[19] This conjecture finds its justification in recent theoretical investigations of electric field induced C-H bond activation in CH_4 in the gas phase. [20] According to these studies, whether C-H bond activation and cleavage may occur following an homolytic or heterolytic regime depends on the nature, orientation and strength of the applied electric field and on how this field will stabilize any of the resonance structures[21, 22] associated with the C-H bond.[8, 23]

We recently qualitatively demonstrated the dual nature of the agostic interactions in intermediates arising in the stereoselective C-H bond palladation[24] of substituted cyclopropyls by using QTAIM[25]-based Noncovalent Interaction (NCI) plots[26] and the DFT-based Extended Transition State – Natural Orbitals for Chemical Valence[27] (ETS-NOCV) orbital interaction decomposition framework.

In this study, we address the CMD/AMLA mechanism of cyclopalladation of *N*,*N*-dimethylbenzylamine[28] from the point of view of non-covalent interactions, by resorting not only to a standard GGA DFT-D3(BJ) method[29] to compute the associated stationary geometries, to the quantum theory of atoms in molecule[25] (QTAIM)-based methods such as the Interacting

[a] *Laboratoire de Mathématiques et de Physique, EA 4217, 52 avenue Paul Alduy, F-66860 Perpignan, France*
[b] *Institut de Chimie de Strasbourg, UMR 7177, 4 rue Blaise Pascal, F-67000 Strasbourg, France.*

† Footnotes relating to the title and/or authors should appear here.
Electronic Supplementary Information (ESI) available: enlarged figure 1b and 2b, Cartesian coordinates (xyz format) of all geometries, total energies and LED terms. See DOI: 10.1039/x0xx00000x

Quantum Atoms[30, 31, 32] (IQA) to investigate in an interatomic wise chemical bond structure changes, but also to the DLPNO-CCSD(T) method, which is also used in combination with the Local Energy Decomposition analysis method[33] to break down NCI components in a fragment-wise fashion in the key intermediates and transition states. Furthermore, we address the effect of the assisting base by comparing the acetate to acetamidate.[34, 35] We also disclose considerations on the fictitious CMD-based cyclonickelation[36, 37] to gauge electrostatic interactions.

Results and discussion

The mechanism of C-H bond activation assisted by an ancillary carboxylate or amidate acting as a base is often invoked in the ortho-palladation of aromatics containing an orienting group. The so-called CMD (or AMLA) mechanism entails three key steps of lower energy payload than the alternative scenario involving an oxidative-addition step of the C-H bond to the metal center.[3, 5, 38] Scheme 1 depicts the CMD mechanism considered throughout this study.

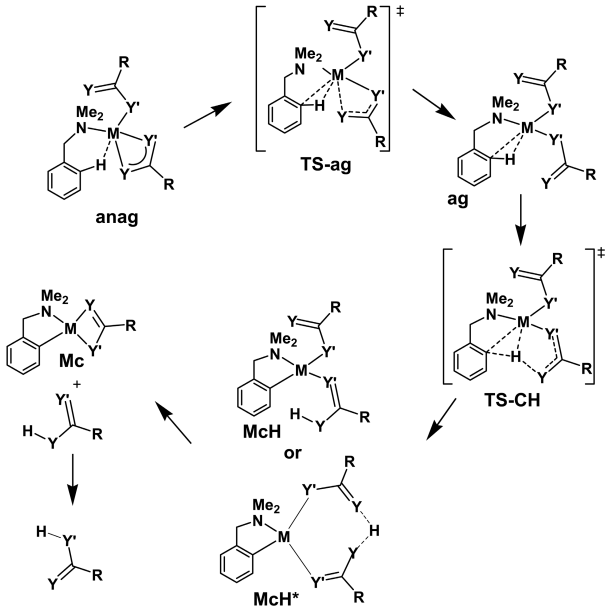

Scheme 1. Mechanism of concerted metallation deprotonation (CMD) considered in this study, where M= Pd or Ni and acetate is considered for Y=Y'=O and acetamidate for Y=O and Y'=NH.

The first step entails the coordination of the "directing group", here a N,N-dimethylamino group, acting as a ligand giving rise assumably to a so-called "anagostic" intermediate, noted **anag** (Scheme 1), where the C-H bond to be activated is generally positioned at ca. 2.7-3.2 Å from the metal centre with no interaction of the latter with the carbon of the C-H motif. The second step entails the dechelation of one the Pd-bound carboxylates leading, via transition state **TS-ag** to the formation of an agostic intermediate **ag** wherein the C-H bond attractively interacts with the metal centre within a multipolar environment where the positioning of the C-H bond close to the vicinal cis carboxylate prefigures the following C-H bond cleavage. The third step, generally occurring with a low barrier of activation, is the C-H bond activation itself that consists of the concerted metallation of the carbon reactive center and the H-atom transfer to the nearby carboxylate via transition state **TS-CH** that leads to the O-protonated acetato metallacycle **McH*** or to **McH** that may hence release the protonated base. A number of reports[5] have addressed the CMD mechanism applied to the cyclopalladation of aromatics , which concluded that the actual energy barrier of the whole process lies in the transition state **TS-ag** of formation of the "agostic" intermediate **ag**, a bottleneck sensitive to steric cluttering. In the present study, our scrutiny has focussed on the states that are most tangibly determining the fate of C-H bond activation, that is **TS-ag**, **ag**, and **TS-CH** for Pd and Ni promoted reactions with the assistance of either acetate AcO^- or of acetamidate $AcNH^-$.

Materials and methods.

For convenience, generic names were given to stationary geometries (Scheme 1). To distinguish each chemical system, a code name is used containing as prefix the metal's chemical symbol **Pd** or **Ni** and as suffix the base , *i.e* **OAc** for acetate and **NHAc** for acetamidate. For the sake of conciseness all energy profiles have been referenced against the Gibbs energy *G* of the **anag** intermediate. All DFT computations have been performed in the gas phase considering exclusively singlet ground and transition states at the generalized gradient approximation (GGA) ZORA-PBE-D3(BJ)/all electron TZP level, which was chosen for the sake of comparison with the recent report of Nielson, Harrison and co-workers.[9] It is worth noting that recent reports by Iron and Janes[39] and Dohm et al.[40] tend to recommend the use of hybrid functionals for a more accurate reproduction of the energetics of reactions, particularly for those involving metal complexes. It is not the purpose of this report to address this issue that deserves a separate study. Finding emerging trends in the role played by non-covalent interactions using differently grounded theoretical frameworks is the main objective of the present study.

Basis set superposition error (BSSE) with the ZORA-PBE-D3(BJ)/all electron triple ζ polarized (TZP) method was previously estimated to represent about less than 3% of the total bonding energy.[41] For safety, a comparison of the interatomic distances in the critical **PdOAc-ag** intermediate in geometries optimized with the ZORA-compliant TZP and the QZ4P basis sets showed significant distance shortening with the larger basis set only for the C_{Ar}-Pd (Δd (TZP-QZ4P)= -0.044 Å) and O_{cis}-Pd segments (Δd (TZP-QZ4P)=-0.025 Å), the remaining key distances within the reactive site viz. C_{Ar}-H_{Ar}, H_{Ar}-Pd, N-Pd, O_{cis}-H_{Ar} varying by less than 0.01 Å.

For the main objective of this study was exclusively to map out intramolecular NCIs that are relevant to the CMD mechanism, implicit "solvation" was not accounted for here: in real systems, solvents (mostly protic) and excess protonated base may interfere with the C-H bond activation step via a Grotthuss-like mechanism[42] of proton capture/relay.[5, 43] This interference of the solvent implies a significant alteration of

the CMD mechanism which is not addressed here and would deserve a distinct study.

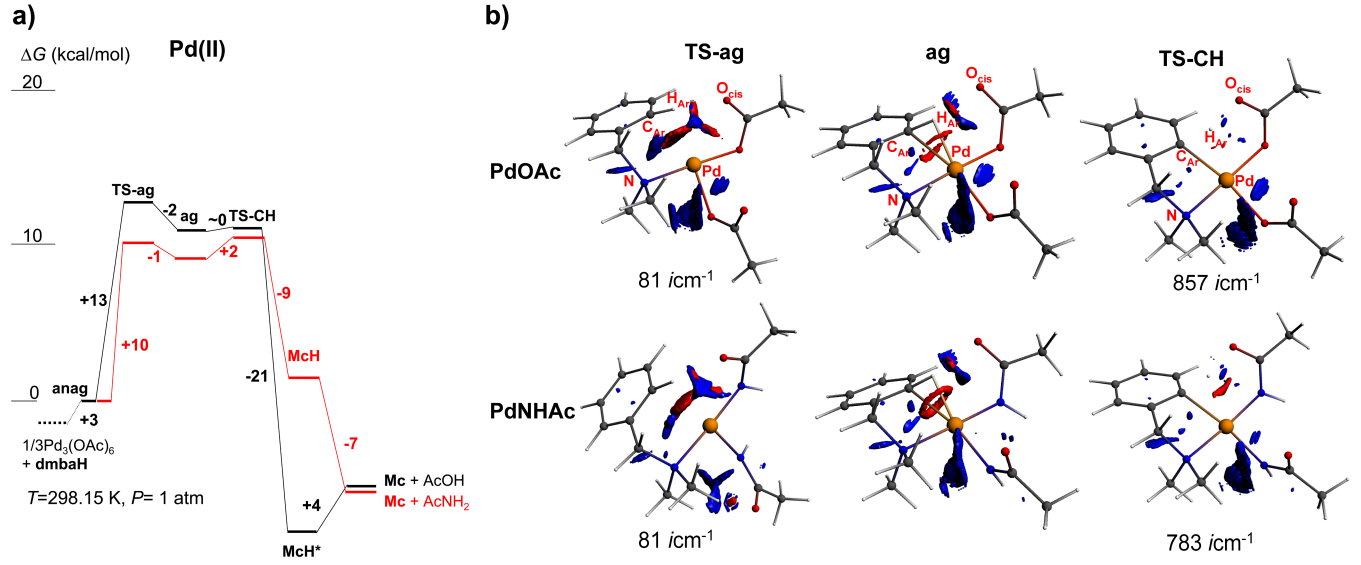

Figure 1. a) Gibbs energy profiles of the cyclopalladation of *N,N*-dimethylbenzylamine (**dmbaH**) in the **PdOAc** (black coloured lines) and **PdNHAc** systems (red coloured lines). b) NCI plots from ADFview2013 for **TS-ag**, **ag** and **TS-CH** in **PdOAc** and **PdNHAc** systems (ZORA-PBE-D3(BJ)/all electron TZP level); NCIs are materialized by reduced density gradient isosurfaces (cut-off value s= 0.02 a.u., ρ= 0.05 a.u.) coloured according to the sign of the signed density $\lambda_2\rho$, i.e in red and blue for attractive and repulsive (or non bonded) NCI domains respectively (cf Supporting Information for larger drawings).

As a consequence the first step of the mechanism that leads to **anag** is given for information only in the **PdOAc** system as basically the dissociation of crown shaped $Pd_3(OAc)_6$ by the *N,N*-dimethylbenzylamine ligand and was not computed in all other cases. In the case of Ni, the **anag** intermediate was assumed to arise from fictitious square-planar singlet state $Ni(OAc)_2$ or $Ni(NHAc)_2$ species. It is indeed known that amidates as ligands favour bridging ligation between two metals or terminal binding through the N atom rather than chelation.[44] It is shown below how this property may play a crucial role.

So-called Bader charges,[25] reduced gradient-based NCI plots[26] and Interaction of Quantum Atoms[30] (IQA) analysis are basis-set independent methods making use of the computed electron density. The QTAIM-based IQA energy partitioning method developed by Pendas and co-workers[30, 31] is a useful tool for investigating interatomic interactions by decomposition into covalent and ionic energy contributions. Based on real-space partitioning of the molecular space, this method, when extended to the Kohn-Sham DFT framework, gives access to a semi-quantitative partitioning of energy contributions of exchange-correlation, and a series of coulombic interaction terms for two-atom interactions within a molecule. The interatomic interaction energy E_{int}^{AB} is the sum of a covalent $E_{covalent}^{AB}$ and an ionic contribution E_{ionic}^{AB}: $E_{int}^{AB} = E_{ionic}^{AB} + E_{covalent}^{AB}$ *with* $E_{ionic}^{AB} = E_{NN}^{AB} + E_{eN}^{AB}[\rho] + E_{Ne}^{AB}[\rho] + E_{eeCl}^{AB}[\rho]$ and $E_{covalent}^{AB} = E_{eeX}^{AB}[\{\psi_i^{KS}\}]$. E_{NN}^{AB}, is the repulsion energy between nuclei in A and B, E_{eN}^{AB} is the attraction of the electrons in A by the nucleus in B, E_{Ne}^{AB} is the reciprocal B electrons attraction with nucleus A and E_{eeCl}^{AB} is the classical electrostatic electronic repulsion energy contribution . The $E_{covalent}^{AB} = E_{eeX}^{AB}[\{\psi_i^{KS}\}]$ is the exchange contribution. The version used in this study that is implemented in ADF[45] v2018, does not consider the semi-empirical dispersion contribution arising from Grimme's Becke-Johnson damped correction[46] accounted for by the PBE-D3(BJ) method. It is nonetheless a useful energy decomposition method for the analysis of multicentre interactions in a multipolar environment (vide infra) where "ionic" and "covalent" contributions are interwoven and delocalized. Here, the IQA analysis is carried out in an atom-pair wise fashion on a selected group of atoms located in what is designated as the reactive site at **TS-ag**, **ag** and **TS-CH**, that is the group of atoms comprising C_{Ar}, H_{Ar}, the metal (Pd or Ni) and O_{cis}.

A wave-function theory-based study has been carried out for these systems using the Domain-based Local Pair Natural Orbital Coupled-Cluster with Single, Double and perturbative Triple excitations[12] (DLPNO-CCSD(T)), starting from the DFT-optimized geometries. The DLPNO-CCSD(T) method combines the high accuracy of the coupled-cluster theory, which is often too computationally demanding for a large system, with a low computational cost, similar to DFT.[47] The reduced computational cost arises from the localisation of the orbitals, constructed at the Hartree-Fock level, and the dichotomy with respect to the inter-orbital distance between "strong" (short distance) and "weak" (long distance) pairs, the latter being treated with a second-order perturbation theory as the pair correlation energy decreases very quickly with the inter-orbital distance. To get a deeper understanding of the role of the different contributions to the energy in the reaction, a Local Energy Decomposition[48] (LED) analysis has been performed. The DLPNO-CCSD(T)/LED method[12] is an efficient, accurate and non-perturbative approach for studying non-covalent interactions, where the localized orbitals are assigned to user-defined fragments, allowing to differentiate between intra- and inter-fragment contributions to the interaction energy, which can then be decomposed into different contributions.

For the LED analysis, localised orbitals obtained from the DLPNO-CCSD(T) calculation are assigned to the different fragments based on Mulliken charges analysis. Thus, in case of a fragmentation where an orbital expands on more than one fragment, it will always be assigned to the fragment with the more electronegative atom involved in this orbital.

The counterpoise correction for the BSSE is here inherently included. Such an approach has already proved useful to enlighten on the importance of London dispersion in the structural stability of agostic complexes.[13]

The interaction energy is decomposed as follows:

$$\Delta E = \Delta E^{HF}_{el-prep} + \Delta E^{C}_{el-prep} + E^{(X,Y)}_{elstat} + E^{(X,Y)}_{exch} + E^{DISP(X,Y)}_{C-SP} + E^{CT(X\rightarrow Y)}_{C-SP} + E^{CT(Y\rightarrow X)}_{C-SP} + E^{(X,Y)}_{C-WP} + E^{(X,Y)}_{C-(T)} + \Delta E_{geo-prep}$$

where $\Delta E^{HF}_{el-prep}$ and $\Delta E^{C}_{el-prep}$ respectively describe the Hartree-Fock (HF) and correlation contribution to the electronic preparation of each of the interacting fragments, $E^{(X,Y)}_{elstat}$ and $E^{(X,Y)}_{exch}$ respectively describe the intermolecular electrostatic and exchange interaction obtained from HF, $E^{DISP(X,Y)}_{C-SP}$, $E^{CT(X\rightarrow Y)}_{C-SP}$ and $E^{CT(Y\rightarrow X)}_{C-SP}$ respectively the dispersion and charge transfer components of the correlation contribution of the strong pairs to the interaction, $E^{(X,Y)}_{C-WP}$ and $E^{(X,Y)}_{C-(T)}$ respectively the corrections to the interaction energy for weak pairs and triple excitations, and $\Delta E_{geo-prep}$ the geometric preparation of the system from the complex to the separated fragments.

For the LED analysis, the studied systems have been subdivided into five fragments. A chemically meaningful fragmentation has been opted for wherever fragments are separated by non-covalent interactions, *viz* the metal centre being fragment **1**, the **dmba** ligand fragment **2** and the two auxiliary basis fragments **3** and **4**. The H_{Ar} being transferred during the reaction from the **dmba** ligand to the auxiliary basis in *cis*, it would change fragment between the **ag** and **McH** steps in the above-mentioned fragmentation. To keep a consistent fragmentation throughout the reaction path, H_{Ar} has been removed from the fragment(**2** or **3**) it is covalently bound to and has been defined as fragment **5**. An illustration of the fragmentation used in this analysis is given in Scheme 2.

It has to be noted that, by construction, the results of the calculations do not depend on the choice of the fragmentation. Test calculations have been run comparing whether H_{Ar} is considered part of fragment **2** or its own single fragment **5**. It appears that contributions involving fragment **2** in the first fragmentation can be retrieved by adding the same contributions involving fragment **2** and fragment **5** in the second. In other words, "superfragments" can be studied by adding the contributions of their constituting fragments. In the following, "superfragments" considered in the study are referred to as the sum of their constituting fragments, *e.g.* "**2+5**" is the fragment consisting in the **dmba** ligand and H_{Ar} (scheme 2). To follow their evolution along the reaction path, every contribution to the interaction energy is given relatively to their value in the **anag** state of the studied system.

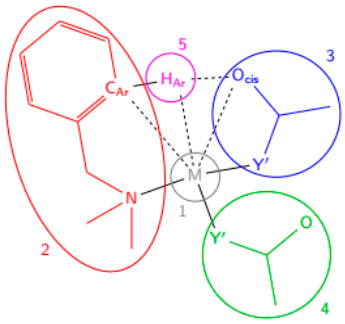

Scheme 2. Illustration of the fragmentation of the system used in the LED analysis considered in this study, where M= Pd or Ni and acetate and acetamidatecorrespond to Y'=O and Y'=NH respectively.

Energy profiles for the CMD mechanisms of cyclopalladation and putative cyclonickelation using acetate and acetamidate as assisting bases. Intermediates and transition states were searched and optimized by standard procedures (Figures 1 and 2), and the Intrinsic Reaction Coordinate (IRC) procedure was used to confirm the direct relationship of each transition state with its related reactant and product. Imaginary frequencies of transition states are provided for information in Figures 1b and 2b. As can be observed in Figure 1a, the energy profile and particularly the energetic barriers for the **PdOAc** system fit well the one originally reported by McGregor and Davies,[3, 5] who used the dispersion correction–devoid GGA BP86 functional.

If one considers the **PdOAc** and **PdNHAc** systems, the barrier to the formation of **ag** is lowered by ca. 3 kcal/mol when acetate is replaced by acetamidate. Relaxation from **TS-ag** to **ag** is isoergonic in the two systems. There is a slightly higher **ag**-to-**TS-CH** barrier in the **PdNHAc** system. Similarly to what McGregor and co-workers reported,[3, 5] in the **PdOAc** system the proton abstracted from the aromatic ligand in **TS-CH** finds its way to a bridging position in between the two off-plane O atoms of the acetato ligands in what is depicted by structure **McH*** (scheme 1), whereas in the **PdNHAc** system, the energy minimum is reached in the **McH** structure where the off-plane O atom of the acetamidato ligand cis to the palladated C atom is protonated.

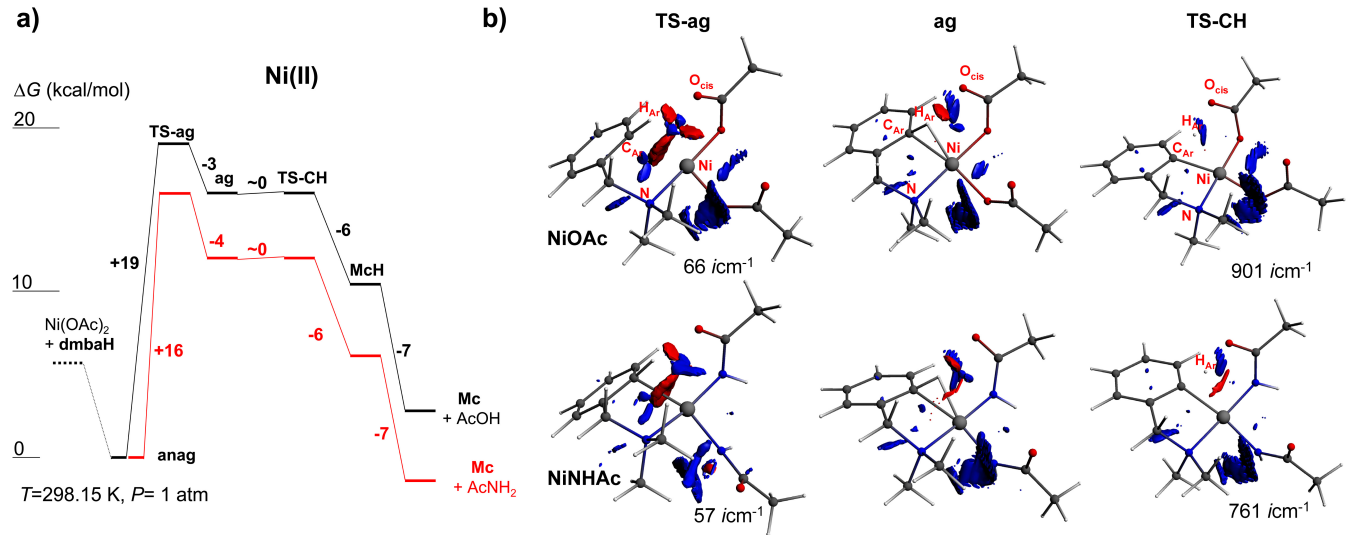

Figure 2. a) Gibbs energy profiles of the cyclonickelation of *N,N*-dimethylbenzylamine (**dmbaH**) in the **NiOAc** (black coloured lines) and **NiNHAc** (red coloured lines) systems (ZORA-PBE-D3(BJ)/all electron TZP level). b) NCI plots from ADFview2013 for **TS-ag**, **ag** and **TS-CH** in **NiOAc** and **NiNHAc** systems (ZORA-PBE-D3(BJ)/all electron TZP level) ; NCIs are materialized by reduced density gradient isosurfaces (cut-off value s= 0.02 a.u., ρ= 0.05 a.u.) coloured according to the sign of the signed density $\lambda_2\rho$, i.e in red and blue for attractive and repulsive (or non bonded) NCI domains respectively (cf Supporting Information for larger drawings).

Table 1. Selected interatomic distances (expressed in Å) and Bader charges in **PdOAc** and **PdNHAc** systems.

entry	system	parameter	**TS-ag**	**ag**	**TS-CH**
1	**PdOAc**	C_{Ar}-H_{Ar}	1.113	1.161	1.354
2		O_{cis}-H_{Ar}	2.066	1.995	1.435
3		Pd-H_{Ar}	2.207	1.875	1.922
4		C_{Ar}-Pd	2.642	2.286	2.121
5		q(C_{Ar})	-0.07	-0.10	-0.22
6		q(H_{Ar})	0.08	0.12	0.32
7		q(Pd)	0.80	0.78	0.75
8		q(N)	-0.77	-0.81	-0.76
9		q(O_{cis})	-1.08	-1.14	-1.04
10	**PdNHAc**	C_{Ar}-H_{Ar}	1.112	1.146	1.323
11		O_{cis}-H_{Ar}	2.113	2.102	1.430
12		Pd-H_{Ar}	2.255	1.935	2.021
13		C_{Ar}-Pd	2.541	2.353	2.161
14		q(C_{Ar})	-0.08	-0.09	-0.26
15		q(H_{Ar})	0.08	0.09	0.33
16		q(Pd)	0.70	0.70	0.67
17		q(N)	-0.79	-0.77	-0.78
18		q(O_{cis})	-1.06	-1.09	-1.02

Overall, the thermochemistry of the **PdOAc** systems is more exergonic than for **PdNHAc** if one considers that significant exergonicity is only achieved by the departure of the O protonated acetamidato ligand that isomerizes into acetamide with the additional release of 7 kcal/mol. The **NiOAc** energy profile (Figure 2a) shows a much larger barrier of activation of 19 kcal/mol for the formation of **ag** via **TS-ag**. This barrier is again lowered down by 3 kcal/mol to 16 kcal/mol in the **NiNHAc** system closer to the one determined for the **PdOAc** system. The relaxation from **TS-ag** to **ag** is equally exoergonic and the transition from **ag** to **McH** via **TS-CH** is nearly barrier-less in the two systems.

The **NiOAc** energy profile (Figure 2a) shows a much larger barrier of activation of 19 kcal/mol for the formation of **ag** via **TS-ag**. This barrier is again lowered down by 3 kcal/mol to 16 kcal/mol in the **NiNHAc** system closer to the one determined for the **PdOAc** system. The relaxation from **TS-ag** to **ag** is equally exoergonic and the transition from **ag** to **McH** via **TS-CH** is nearly barrier-less in the two systems.

Table 2. Selected interatomic distances (expressed in Å) and Bader charges in **NiOAc** and **NiNHAc** systems.

entry	system	parameter	**TS-ag**	**ag**	**TS-CH**
1	**NiOAc**	C_{Ar}-H_{Ar}	1.117	1.179	1.379
2		O_{cis}-H_{Ar}	2.044	1.910	1.391
3		Ni-H_{Ar}	1.985	1.715	1.805
4		C_{Ar}-Ni	2.353	2.048	1.954
5		q(C_{Ar})	-0.10	-0.14	-0.26
6		q(H_{Ar})	0.08	0.11	0.32
7		q(Ni)	0.94	0.91	0.89
8		q(N)	-0.88	-0.80	-0.80
9		q(O_{cis})	-1.09	-1.08	-1.02
10	**NiNHAc**	C_{Ar}-H_{Ar}	1.126	1.168	1.331
11		O_{cis}-H_{Ar}	2.027	1.918	1.405
12		Ni-H_{Ar}	1.990	1.771	1.892
13		C_{Ar}-Ni	2.271	2.095	1.991
14		q(C_{Ar})	-0.10	-0.15	-0.28
15		q(H_{Ar})	0.08	0.12	0.33
16		q(Ni)	0.85	0.81	0.81
17		q(N)	-0.82	-0.83	-0.80
18		q(O_{cis})	-1.08	-1.07	-1.01

NCI plots and Bader charges. The way NCI plots are depicted in Figures 1b and 2b distinguishes attractive domains (red coloured isosurfaces) from repulsive or non-bonded ones (blue colored isosurfaces). Quite interestingly, all four NCI plots for the **TS-ag** transition states in Figures 1b and 2b show a three-leaf clover shaped attractive NCI domain in the reaction site that is consistent with the transformation undergoing on the way towards the metastable **ag** intermediate: the chelation by the base cis to **dmbaH** recedes to the establishment of the agostic C-H-metal interaction. The attractive component located in the metal-$C_{Ar}H_{Ar}$, metal-O_{cis} and H_{Ar}-O_{cis} segments is consistent with the large electrostatic attraction between C_{Ar} and the metal suggested by the values of charges of opposite sign already pointed out in recent[9, 10] reports.

Table 1 lists Bader charges[25] q for a selection of atoms and interatomic distances for the key C_{Ar}-H_{Ar}-Pd-O_{cis} motif that comprises the C-H bond to be activated, the palladium centre and the off-plane O atom of the *cis* acetato or acetamido ligands in **TS-ag**, **ag** and **TS-CH** geometries for the **PdOAc** and **PdNHAc** systems.

Table 2 lists Bader charges[25] q for a selection of atoms and interatomic distances for the key C_{Ar}-H_{Ar}-Ni-O_{cis} motif that comprises the C-H bond to be activated, the nickel centre and the off-plane O atom of the *cis* acetato or acetamido ligands in **TS-ag**, **ag** and **TS-CH** geometries for the **NiOAc** and **NiNHAc** systems. Note that the H_{Ar}-Ni and C_{Ar}-Ni distances of both **NiOAc-ag** (Table 2, entry 3 and 4) and **NiNHAc-ag** (Table 2, entry 12 and 13) are consistent, although by ~0.3 Å shorter, with those determined by X-ray diffraction analysis by van der Vlugt and co-workers[37] for a phosphonito pyridylphenyl Ni agostic complex wherein the Ni centre is constrained by chelation to the ditopic phosphinitopyridyl moiety (C_{Ar}-Ni 2.355(8) Å, H_{Ar}-Ni 2.02(9) Å).

As a matter of fact from the view point of the C-H bond activation **TS-ag** prefigures the multipolar environment by which the C_{Ar}-H_{Ar} bond is surrounded all the way till **TS-CH**. In intermediate **ag,** in all four considered systems, attractive NCI isosurfaces are present in the H_{Ar}-O_{cis} segment as a symptom of a significant coulombic interaction. Again the values of $q(O_{cis})$ and $q(H_{Ar})$ support a dominant ionic character for this attractive NCI. Though, one interesting feature is the attractive NCI ring structure observed in **PdOAc-ag** , **PdNHAc-ag** and **NiNHAc-ag** that is generally symptomatic of the existence of a weak C-H σ-to- metal d orbital charge transfer interaction, already reported in a previous study.[34] QTAIM investigations (not shown here) confirm indeed the existence of a bond critical point (3,-1) and a bond path for the metal-C_{Ar} interaction.

In **TS-CH**, the NCI plots do not reveal major attractive domains. The one located in the H_{Ar}-O_{cis}-metal triangle in **PdNHAc** (Figure 1b) and **NiNHAc** (Figure 2b) can seemingly be assigned to the coulombic attraction operating between O_{cis} and the metal centre according to the rather high difference of atomic charge $q(O_{cis})$ and q(Pd or Ni) (entries 18 in Tables 1 and 2).

Bader charges indicate clearly that the Pd centre is less positively charged than the Ni one in related **PdOAc**/**NiOAc** and **PdNHAc**/**NiNHAc** systems (Table 1 and 2, entry 7).

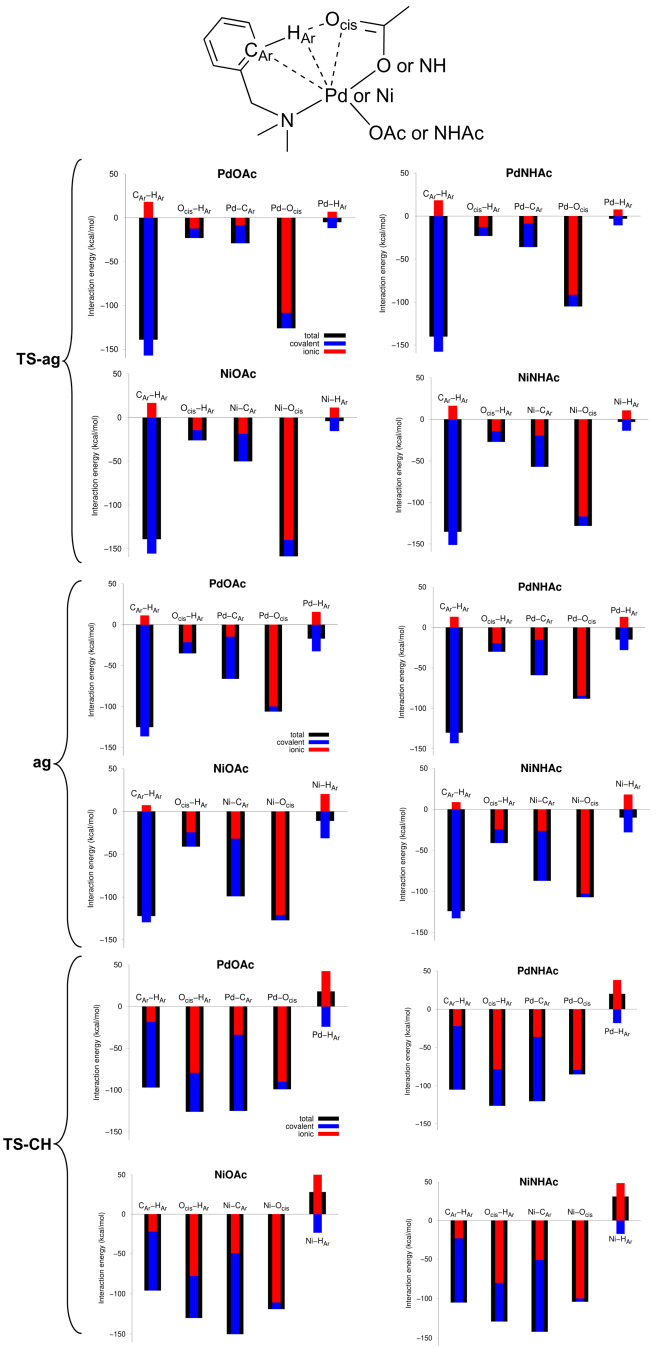

Figure 3. IQA analysis of **TS-ag**, **ag** and **TS-CH** in **PdOAc**, **PdNHAc**, **NiOAc**, **NiNHAc** systems. Histogram of atom-pair interaction energies within the reactive site (black coloured, total E_{int} in kcal/mol) are decomposed into their covalent component (blue coloured bars) and ionic component (red coloured bars) (cf ESI for an alternative presentation).

It is also evident that the positive charge of H_{Ar} increases steadily on going from **TS-ag** and **ag** to **TS-CH**, i.e. from a value close to neutrality in the former two states to a value of ca. +0.3 in the latter (Table 1 and 2, entry 6). This suggests a rather strong repulsion between the metal center and this hydrogen atom in **TS-CH**, a stage where, like shown in the

following, the C_{Ar}-H interaction contains an enhanced ionic character although not dominant.

Interacting Quantum Atoms analysis. As stated above the IQA investigation focussed essentially on the main atoms of the reactive site that embraces a part of the atoms bonded to the metal centre. Figure 3 gives the details of the pair-wise interatomic interaction energies E_{int} for the reactive site with the respective covalent and ionic contributions expressed as a percentage of E_{int} for the three key situations **TS-ag**, **ag** and **TS-CH** in **PdOAc**, **PdNHAc**, **NiOAC** and **NiNHAc** systems. Negative percentages apply to the E_{int} value and mean that the contribution in question opposes to the dominant one.

The consistency of the values of E_{int} with the chemical reaction of interest can be confirmed by looking at the decreasing E_{int} values for interatomic interaction undergoing the greatest changes. For example, the C_{Ar}-H_{Ar} interaction energy in **PdOAc** decreases from a value of -139 kcal/mol in **TS-ag** to -97 kcal/mol in **TS-CH**. The same variation is observed for **NiNHAc**, with a decrease from -135 to -105 kcal/mol. The turning point for the ionic interaction contribution to E_{int} for the C_{Ar}-H_{Ar} interaction is **TS-CH** where its energy share becomes constructive (same sign as the covalent); from a valence bond theory viewpoint it could be related to an increased "weight" of the $C_{Ar}^{-}H_{Ar}^{+}$ resonance structure.[21]
For the H_{Ar}-metal interaction in **PdOAc**, E_{int} evolves from a slightly "attractive" value of ca. -5 kcal/mol in **TS-ag** to a value of -17 kcal/mol in **ag**, and abruptly reverses into a repulsive interaction with a value of +18 kcal/mol in **TS-CH**. This trend that is observed also in **PdNHAc**, **NiOAc** and **NiNHAc** corresponds to a progressive weakening of the covalent H_{Ar}-metal component already poised by a strong ionic repulsive contribution in **TS-ag** and **ag** that eventually dominates in **TS-CH**. Quite consistently the C_{Ar}-metal interaction, that is built of two constructive covalent and ionic contributions of the same sign in a ~ 7:3 ratio, is strengthened (increasing absolute value of E_{int}) along the energy path as this interaction gets closer to an exclusive C_{Ar}-metal bond. This E_{int}(H_{Ar}-M) interaction energy reversal that occurs from **ag** to **TS-CH** corresponds to interatomic excursions for the C_{Ar}-H_{Ar}, H_{Ar}-O_{cis} and H_{Ar}-M distances of ca. +0.20, -0.55 and +0.10 Å, which in almost all cases but **PdNHAc** requires a negligible Gibbs energy payload at this level of theory (GGA DFT-D).

The situation around O_{cis} deserves a special attention. This oxygen atom that was previously bound to the metal in **anag** still preserves a reasonable attractive ionic interaction with it in **TS-ag**, **ag** and **TS-CH**. The value of E_{int} for the O_{cis}-Pd interaction evolves in **PdOAc** steadily from -126 to -106 kcal/mol in **TS-ag** and **ag** to a value of -99 kcal/mol in **TS-CH**. This clearly indicates that the acetate ligand is not plainly monodentate in **ag**, this up to the passing of **TS-CH** where this partial chelation situation is lifted by the capture of H_{Ar}. The comparison of acetato and acetamidato systems informs that the value of E_{int} for the O_{cis}-metal interaction is by 20 to 30 kcal/mol lower in absolute value in **PdNHAc-TS-ag** and **NiNHAc-TS-ag** whereas E_{int} for the H_{Ar}-O_{cis} interaction is nearly identical in all four systems. It can be speculated that the lowering of the barrier of activation for the formation of **ag** in **PdNHAc** and **NiNHAc** is rooted in the lower residual chelation of the metal by the cis acetamidate ligand.

DLPNO-CCSD(T)/LED investigation. Intermediates and transition states that have been optimized above were studied using the DLPNO-CCSD(T)/LED approach. After a user-defined fragmentation of the system, Hartree-Fock and correlation energies were differentiated between intra- and inter-fragment contributions to the interaction energy and further decomposed into electronic promotion, electrostatic, exchange, dynamic charge polarization, and dispersion contribution (see supporting information for detailed LED energy terms).

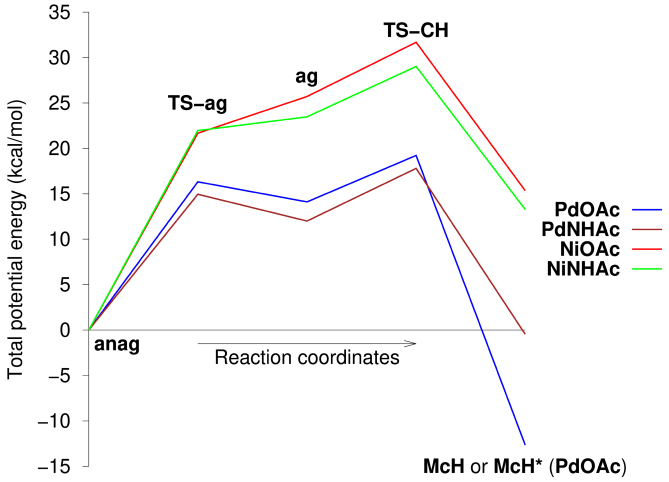

Figure 4. Total potential energy profile computed at the DLPNO-CCSD(T)/def2-TZVP level from the DFT-optimized geometries. Energies are expressed relative to **anag**.

Considering the **PdOAC** and **PdNHAc** systems, the energy barrier to formation of **ag** is here slightly lowered when replacing acetate by acetamidate, while the relaxation from **TS-ag** to **ag** and the **ag**-to-**TS-CH** barrier are slightly lowered. In the case of the Ni analogues, the **TS-ag**-to-**ag** step is endoenergetic and is lowered by *ca.* 2 kcal/mol when replacing acetate by acetamidate, while the **ag**-to-**TS-CH** barrier is slightly lowered (by less than 1 kcal/mol). For both the acetate and acetamidate, the **anag**-to-**TS-ag** step is less endoenergetic for the Pd analogues than for the Ni one; but the **ag**-to-**TS-CH** step is lower in energy for **PdOAc** than for **NiOAc**, while it is higher for **PdNHAc** than for **NiNHAc**.
From the construction of the fragmentation (scheme 2), the interaction energy between fragment **5** and any other fragment is purely electrostatic in nature as no orbital was assigned to fragment **5** in the computation, for H_{Ar} has a lower electron population than the other atom(s) it bound to (C_{Ar} or O_{cis}) in the orbital it is involved in. For the four considered systems, the population on H_{Ar} in the orbital it is involved in with C_{Ar} decreases from around 40 % at **anag** to 10-15 % in **TS-CH** where the electron population is similar to the one in the orbital it is involved with O_{cis}, which increases to around 30 % in **McH** (or **McH*** in **PdOAc**). Also, at **ag**, the distribution of the population in the orbital involving H_{Ar} is of the order of 60 %

on C_{Ar}, 30 % on H_{Ar} and 10 % on the metal, which supports the hypothesis of the agostic bond having some 2 electron-3 center character. So, as no orbital is assigned to fragment **5**, all the information about the exchange and correlation around the reactive center is included in the interactions between fragments **1**, **2**, and **3**, while fragment **5** gives a deeper insight on the electrostatic behaviour around the reactive center.

The interaction energy between fragments **1** and **5** (Figure 5a) is therefore repulsive all along the reaction path and increases continuously from **anag** to **ag** and decreases continuously from **ag** to **McH** (or **McH***) for the four considered systems (Figure 5a). The repulsion barrier between fragments **1** and **5** is lowered when acetate is replaced by acetamidate (Figure 5a, 8 kcal/mol for Pd, and 10 kcal/mol for Ni). The interaction energy between fragments **2** and **5** is attractive all along the reaction path and decreases continuously (Cf Supporting Information Figure S9), while the interaction energy between fragments **3** and **5** is attractive all along the reaction path and continuously decreases (cf. Supporting Information Figure S9), describing the transfer of the proton H_Ar from the dmba to the base in cis, whith the interaction between H_Ar and both fragments always being stabilizing.. The sum of these two contributions (interaction between H_{Ar}, and C_{Ar} and O_{cis} in their respective fragments, *i.e.* between fragment **5** and "superfragment" **2+3**) continuously decreases from **anag** to **ag** then continuously increases from **ag** to **McH** (or **McH***), defining the agostic intermediate **ag** as a minimum of the interaction energy of the reactive system base-**dmba** (Figure 5c). The decrease in this energy for the formation of **ag** represents between 40% (for **PdNHAc**) and 47% (for **NiOAc**) of the barrier height in the interaction energy between **1** and **5**, this percentage decreases by 3% when acetate is replaced by acetamidate, for both metals. In both case, this decrease arises from an increase of the barrier height of about 10 kcal/mol and a decrease of the well depth of about 7 kcal/mol.

The interaction energy between fragments **1** and **2** is attractive all along the reaction path and decreases continuously along the reaction path (see Figure S3 in the Supporting Information)for each of the considered systems (cf. ESI). The same trend is followed by the electrostatic, exchange, and correlation contributions. The electrostatic contribution represents in average 92 % of the interaction energy for the Ni analogues and 89 % for the Pd analogues, all being maximal at **TS-ag** and minimal at **McH** (or **McH*** for **PdOAc**). The correlation contribution to the interaction energy ranges between 2 % and 3 % for all systems, around 40 % of which are due to dispersion.

On the opposite, the interaction energy between fragments **1** and **3** is attractive all along the reaction path and continuously increases (see Figure S4 in the Supporting Information), except for **NiNHAc** where it decreases from **TS-ag** to **ag** before increasing again and for **PdNHAc** where it decreases from **anag** to **TS-ag** before increasing. The electrostatic (Figure 5b), exchange, and correlation contributions follow the same trends.

The interaction energy between fragments **1** and **4** (see Figure S5 in the Supporting Information) is attractive all along the reaction path and decreases from **anag** to **TS-ag** to **ag** then increases from **ag** to **TS-CH** to **McH**, except for **NiOAc** for which it continuously increases (cf. ESI). The same trends are followed by the electrostatic contribution. Exchange contributions follow the trends in the case of **PdNHAc** and **NiOAc**, but in the case of **NiNHAc** and **PdOAc** it increases from **TS-ag** to **ag**.

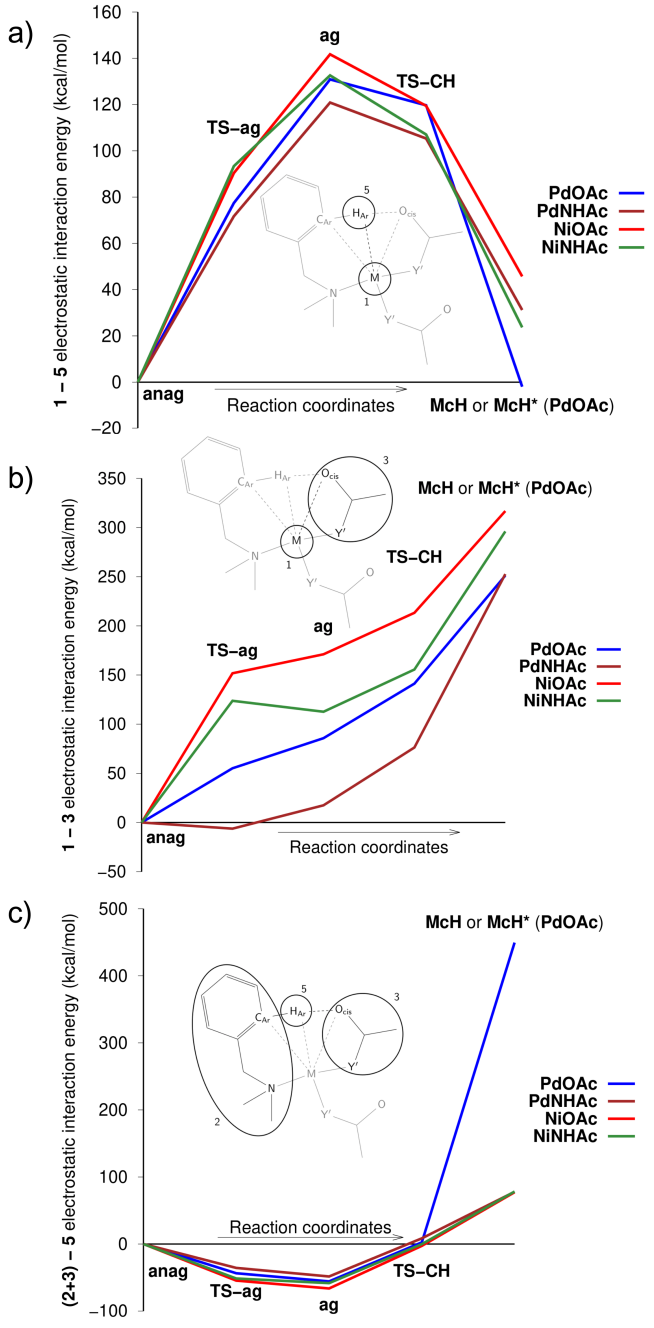

Figure 5. Electrostatic interaction energy plot along the reaction path for interfragment interactions **1**-**5** (a) and **1**-**3** (b) and the total interaction energy for the interfragment interaction (**2**+**3**)-**5, which** shows an electrostatic interactions minimum at **ag** for the four systems.

Correlation contributions decrease from **anag** to **TS-ag** then continuously increase for all systems (cf. ESI). Dispersion contributions continuously increase along the reaction path for all systems. The electrostatic contribution represents in

average 92 % of the interaction energy for the Ni analogues and 90 % for the Pd analogues, this contribution being lowered by almost 1 % when acetate is replaced by acetamidate. The correlation contribution to the interaction energy ranges between 2 % and 3 % for all systems, around 30 % of which are due to dispersion for the Pd analogues and 25 % of which for the Ni analogues. The interaction energy between fragments **2** and **3** (see Figure S6 in the Supporting Information) is attractive all along the reaction path and increases continuously from **anag** to **ag** then decreases from **ag** to **TS-CH** before increasing again from **TS-CH** to **McH** for the four considered systems, note that the **TS-ag**-to-**ag** step is quasi-isoenergetic for the Ni analogues. The electrostatic contributions continuously increase from **anag** to **ag** then decrease from **ag** to **McH**. The exchange and correlation contributions continuously decrease from **anag** to **TS-CH** then increase from **TS-CH** to **McH**. The dispersion contributions follow the same trend when acetamidate is the auxiliary base, but increase from **anag** to **TS-ag** for the acetate analogues. The electrostatic contribution to the interaction energy is also repulsive and represents 110 % to 115 % of the interaction energy from **anag** to **ag** then increases to 137 % for **PdOAc,** 138 % for **PdNHAc** and 140 % for the Ni analogues at **TS-CH** then decreases again at **McH** (or **McH*** for **PdOAc**). The exchange and correlation contributions are, on the contrary, attractive. The correlation contribution ranges between -5 % and -8 % of the interaction energy from **anag** to **ag** then increases to -14 % for the Pd analogues and -15 % for the Ni analogues. The dispersion contribution decreases from around 50 % of the correlation contribution in **anag** to 27-28 % at **TS-CH** then decreases again, for all studied systems.

The total interaction energy (sum over all interactions) is attractive all along the reaction path and continuously decreasing all along the reaction path (see Figure S10 in the Supporting Information), except for **NiOAc** for which a barrier of 29 kcal/mol appears for the formation of the agostic intermediate **ag**. For both Pd and Ni, the total interaction energy is lower for the acetamidate analogue than for the acetate one until the formation of **ag**, and becomes higher until the formation of **McH** (or **McH***). The same trends are followed by the total electrostatic interaction and the total exchange interaction contributions. The total correlation interaction contribution is, for all four systems, continuously decreasing from **anag** to **TS-CH** and then increases towards **McH** (or **McH***). The total dispersion interaction contribution continuously decreases all along the reaction path for the acetamidate analogues, but presents a barrier for the formation of the agostic intermediate **ag** for both acetate analogues (0.4 kcal/mol for **PdOAc** and 0.2 kcal/mol for **NiOAc**).

Contributions of the different inter-fragment interactions to the total interaction energy are given in Table 3. The contribution to the total interaction energy only varies significantly for five fragment-pairs: **1**-**2**, **1**-**3**, **1**-**4**, **2**-**5** and **3**-**5**. The main contribution is the **1**-**3** interaction at **anag** for the acetate analogues and at **anag** and **TS-ag** for the acetamidate analogues, and the **1**-**2** interaction for all other geometries, these two contributions remain the two main ones during the whole reaction for all four systems. The **1**-**2** interaction contribution increases and the **1**-**3** interaction contribution decreases through the whole reaction, describing respectively the metal-C_{Ar} bond formation and the metal-O_{cis} bond breakage..

Table 3. Contributions (in percentage) of the different inter-fragment interaction energies to the total interaction energy as generated by the LED method from DLPNO-CCSD(T) computations.

system	state	1-2	1-3	1-4	1-5	2-3	2-4	2-5	3-4	3-5	4-5
PdOAc	**anag**	28	32	27	-8	-5	-3	26	-4	5	3
	TS-ag	33	29	28	-11	-5	-4	26	-5	6	3
	ag	39	26	26	-12	-5	-4	24	-4	6	4
	TS-CH	46	23	23	-11	-4	-4	18	-4	10	3
	McH*	63	17	12	-7	-4	-3	3	-3	8	13
PdNHAc	**anag**	23	34	31	-8	-5	-2	24	-4	5	3
	TS-ag	27	33	30	-10	-5	-3	23	-4	6	3
	ag	31	31	30	-11	-5	-4	22	-4	6	3
	TS-CH	37	29	27	-10	-4	-4	16	-4	10	3
	McH	51	22	20	-8	-5	-3	6	-3	18	3
NiOAc	**anag**	27	34	27	-8	-5	-3	24	-4	4	3
	TS-ag	34	29	28	-11	-6	-3	25	-4	6	3
	ag	42	26	25	-12	-5	-4	22	-4	6	3
	TS-CH	47	23	23	-11	-4	-3	16	-3	10	3
	McH	55	19	19	-9	-5	-3	6	-3	17	3
NiNHAc	**anag**	23	36	30	-8	-4	-2	22	-4	4	3
	TS-ag	30	31	30	-10	-5	-3	22	-4	6	3
	ag	35	30	28	-11	-5	-3	20	-3	6	3
	TS-CH	39	28	26	-10	-4	-3	15	-3	9	3
	McH	48	23	22	-8	-4	-3	5	-4	16	3

The contribution of the **1**-**4** interaction follows the same variation than the **1**-**3** interaction, meaning that the interaction between the metal and both auxiliary bases varies in the same way but for different reasons: the 1-3 interaction contribution decreases because of the cleavage of the metal-base bond, while the 1-4 interaction contribution decreases because of the trans influence of the formation of the metal-aryl bond. Contributions from **2**-**5** and **3**-**5** vary in opposite: being both rather constant from **anag** to **ag**, the contribution of **2**-**5** decreases while the contribution of **3**-**5** increases, which illustrates that the cleavage of the C_{Ar}-H_{Ar} bond in favor of the formation of the O_{cis}-H_{Ar} bond only takes place after the **ag** step.. The sum of the contributions of **2**-**5** and **3**-**5** interactions is almost constant throughout the reaction for the acetamidate analogues, while it decreases from **ag** to **McH** or **McH*** for the acetate analogues.

General Discussion. The two methods consistently produce a higher energy payload (defined here as the energy required to pass the highest transition state starting from the initial reference state) for cyclonickelation as compared to cyclopalladation. Overall the total electronic energy payload for the **anag**-to-**McH***/**McH** at the DLPNO-CCSD(T) level is ca. 30 and 18 kcal/mol for the Ni and Pd systems whereas at the GGA PBE-D3(BJ) level the payload amounts respectively ca. 17 and 12 kcal/mol in total electronic energy. Compared to the GGA PBE-D3 energy profiles for the four systems, the DLPNO-CCSD(T) ones give higher barriers of activation for the **ag**-to-**McH** (or McH*) step. This major difference lies in the more accurate physical description[49] of the proton transfer process *via* **TS-CH** by the DLPNO-CCSD(T) method. The systematic underestimation by DFT[50] of proton transfer barriers stems from the self-interaction[51] effect that reportedly tends to stabilize delocalized states such as **TS-CH**.[47,48] Therefore this higher DLPNO-CCSD(T) barrier, which is about less than twice as large for the Ni than for the Pd systems (as compared to the quasi "barrierless" **ag**-to-**McH***/**McH** process computed at the PBE-D3(BJ) level), is rather critical.

It is evident from Figure 5c that all the GGA DFT-D optimized geometries of **ag** used in this study give rise to a minimum value for the interfragment interaction energy between superfragment (**2**+**3**) and **5**, thus suggesting that the **ag** geometries used in the calculations are rather close to a local energy minimum at the DLPNO-CCSD(T) level.

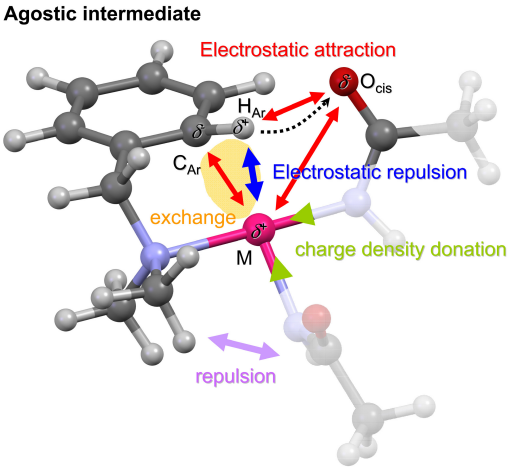

Figure 6. Summary of the effects governing the reactivity of the **ag** intermediate in the CMD mechanism. Colour code for unshaded atoms: blue N, dark grey C, light grey H, red O, magenta metal. Red and blue arrows depict attractive and repulsive electrostatic interactions respectively. Charge density donation from the auxiliary bases is drawn in green. The egg-shaped orange-yellow area depicts the weak exchange C_{Ar}-H_{Ar}-metal interaction.

Overall the CMD mechanism applied to the cyclopalladation and cyclonickelation of *N,N*-dimethylbenzylamine shows a major sensitivity to electrostatic repulsion (Figure 6). The latter is indeed largely rooted in the nature of the metal; the Ni centre displaying overall a larger positive charge than Pd, which results in a larger barrier to formation of the agostic intermediate **ag**.

Also of importance is the nature of the auxiliary base. In the Ni and Pd systems the acetamidato ligands lower the **anag**-to-**ag** and the **ag**-to-**McH***/**McH** barriers. This effect seems to be essentially due to the inherently lower chelating property of the acetamidato ligand and the lower electrostatic repulsion between the C_{Ar}-H_{Ar} bond and the metal induced by charge density donation to the metal from the two acetamidato N ligands. In other terms, the interaction of the carboxy unit C(O) of the base with H_{Ar} is not exclusive in **ag**: a significant residual ionic interaction exists between the cis-located base and the metal centre in all four systems, which competes with the proton transfer process that appears now to be rather sensitive to the effective charge lying at O_{cis}.

Nonetheless, in the **PdNHAc** and **NiNHAc** systems, the residual chelation of the cis acetamido ligand is significantly lower than in the **PdOAc** and **NiOAc** systems: it seems that significant improvement of the feasibility of the CMD mechanism with first row metal complexes lies, among other issues, in the judicious choice of the auxiliary base that should be a ligand with the lowest propensity for chelation and the strongest ligand to metal σ-donating properties in its monohapto mode. The sensible decrease of the charge at the metal upon substitution of AcO^- for $AcNH^-$ contributes indeed to the decrease of the electrostatic repulsion between the metal and H_{Ar}, which persists nonetheless throughout the process and is particularly acute in the **ag**-to-**TS-CH** step involving proton transfer and carbometallation. Finally, it must be pointed out according to DLPNO-CCSD(T) calculations that the interfragment interactions **2**-**4** corresponding to the **dmba**-to-*trans*-base interaction is increasingly repulsive (total energy) from **anag** to **ag** in the four studied systems (cf. ESI). We speculate that minimizing this repulsive contribution of the non-reactive trans-base (fragment 4, scheme 2) by its replacement by a donating anionic ligand of smaller size than AcO^- could improve significantly the cyclometallation process.

Conclusions

In this study, the CMD/AMLA mechanism of cyclopalladation and cyclonickelation has been investigated by joint DFT-D and DLPNO-CCSD(T) methods assisted by QTAIM-IQA and LED analytical procedures to map out the role of NCIs in the key stages of the reaction. The study points the crucial role played by electrostatic interactions, which somewhat govern the whole process that is very sensitive to the charge borne by the metal centre. This is expressed by a larger energy payload for the formation of the pivotal Ni-**ag** transient (as compared to Pd-**ag**) but also by a larger activation barrier for the final C-H bond carbometalation/deprotonation step (**ag** to **McH**/**McH***) of the CMD mechanism. In line with previous reports on the CMD mechanism,[3-5, 9, 10, 52] this study suggests that the formation of an agostic intermediate is not only crucial but must occur within a proper multipolar environment around the C-H bond, to enhance the feasibility of the whole carbometallation deprotonation process. It is found that

substitution of acetate for acetamidate as the auxiliary base and ligand should improve the efficiency of the cyclometallation reaction[34, 35] owing to lower propensity of the latter base to maintain a residual chelation with the metal centre. Finally, on a wider scope, the possibility of proton-relay effects operating during the cyclometallation reaction[5, 43] advocates the inclusion of both explicit and implicit solvation effects particularly with polar protic solvents or reagents as they may actively influence the whole reaction energy profile and modify the structure of the key intermediates and transition states. This aspect of utmost importance, which was eluded in this work is to be addressed in future studies and will be reported on in due time.

Computational details. Geometry optimizations of reactants, intermediates, transitions states and products were performed with the methods of the density functional theory using the SCM-ADF[45]2018.01 package, considering the molecules in the gas phase at the singlet state. The PBE[53] functional augmented with Grimme's DFT-D3(BJ) implementation of dispersion with a Becke–Johnson (BJ) damping function[46] was used in all geometry optimizations. All computations were carried out using scalar relativistic corrections within the zeroth order regular approximation for relativistic effects with *ad hoc* all-electron (abbreviated ae) single polarization function triple-ζ Slater type basis sets (TZP).[54] Geometry optimizations by energy gradient minimization were carried out in all cases with integration grid accuracy comprised between 4.5 and 6.5, an energy gradient convergence criterion of 10^{-3} au, and a tight to very tight SCF convergence criterion. All transition states were submitted to the Intrinsic Reaction Coordinate (IRC) procedure to verify the connection to their reactive complexes and products. Counterpoise correction for basis set superposition error (BSSE) was neglected throughout this study. Vibrational modes were analytically computed to verify that the optimized geometries were related to energy minima or to transition states. Bader (QTAIM) charges[25] and Interacting Quantum Atoms analyses[30, 31] (IQA) were carried out using the embedded QTAIM functionalities of the ADF package. For technical reasons regular all electron TZP Slater type basis sets for all elements except for Pd, for which a basis set with a frozen core up to 3*d* was used for IQA. Drawings of molecular structures and isosurfaces were produced with ADFview2018.
For each of the four studied system, DLPNO-CCSD(T)[12] calculations with the TightPNO threshold on the PBE-D3(BJ) optimized geometries for **anag**, **TS-ag**, **ag**, **TS-CH** and **McH** were performed using the ORCA program system[55]version 4.1.1. The balanced Karlsruhe 2nd generation default triple-ζ valence plus polarization (def2-TZVP) basis set[56] was used in these calculations, as well as automatically generated auxiliary basis set.[57] The LED analysis[48] has been performed to quantify the different intra- and inter-fragment contributions to the energy. For this analysis, each system has been subdivided into five fragments : the metal center, the transferred H_{Ar}, each auxiliary base and the **dmba** ligand from which the H_{Ar} *ortho* to the *N,N*-aminomethyl group has been removed.

Conflicts of interest

There are no conflicts to declare

Acknowledgements

The authors gratefully acknowledge the support provided by the Centre National de la Recherche Scientifique and the University of Strasbourg. Prof Dr Gerard van Koten and Dr Michel Pfeffer are gratefully acknowledged for fruitful discussions.

Notes and references

1. N. Kuhl, M. N. Hopkinson, J. Wencel-Delord and F. Glorius, *Angew. Chem., Int. Ed.*, 2012, **51**, 10236-10254; C. Sambiagio, D. Schönbauer, R. Blieck, T. Dao-Huy, G. Pototschnig, P. Schaaf, T. Wiesinger, M. F. Zia, J. Wencel-Delord, T. Besset, B. U. W. Maes and M. Schnürch, *Chem. Soc. Rev.*, 2018, **47**, 6603-6743; P. Gandeepan, T. Müller, D. Zell, G. Cera, S. Warratz and L. Ackermann, *Chem. Rev.*, 2019, **119**, 2192-2452.
2. D. Zell, M. Bursch, V. Müller, S. Grimme and L. Ackermann, *Angew. Chem. Int. Ed.*, 2017, **56**, 10378-10382; J. Ghorai and P. Anbarasan, *Asian J. Org. Chem.*, 2019, **8**, 430 -455; J. Wencel-Delord, T. Dröge, F. Liu and F. Glorius, *Chem. Soc. Rev.*, 2011, **40**, 4740-4761; J. Wencel-Delord and F. Glorius, *Nature Chem.*, 2013, **5**, 369.
3. D. L. Davies, S. M. A. Donald and S. A. Macgregor, *J. Am. Chem. Soc.*, 2005, **127**, 13754-13755.
4. Y. Boutadla, D. L. Davies, R. C. Jones and K. Singh, *Chem. Eur. J.*, 2011, **17**, 3438-3448.
5. D. L. Davies, S. A. Macgregor and C. L. McMullin, *Chem. Rev.* , 2017, **117**, 8649-8709.
6. C. He, M. Hou, Z. Zhu and Z. Gu, *ACS Catalysis*, 2017, **7**, 5316-5320; C. K. Hazra, Q. Dherbassy, J. Wencel-Delord and F. Colobert, *Angew. Chem. Int. Ed.*, 2014, **53**, 13871-13875; C. Wang, I. Piel and F. Glorius, *J. Am. Chem. Soc*, 2009, **131**, 4194-4195; M. Lautens and C. Dank, *Synfacts*, 2018, **14**, 1256.
7. M. Brookhart and M. L. H. Green, *J. Organomet. Chem.*, 1983, **250**, 395-408; M. L. H. Green and D. O'Hare, *Pure Appl. Chem.*, 1985, **57**, 1897-1910; M. Brookhart, M. L. H. Green and G. Parkin, *Proc. Nat. Acad. Sci. USA*, 2007, **104**, 6908-6914; F. A. Cotton, *Inorg. Chem.*, 2002, **41**, 643-658; G. F. Schmidt and M. Brookhart, *J. Am. Chem. Soc*, 1985, **107**, 1443-1444; W. Scherer, V. Herz, A. Brück, C. Hauf, F. Reiner, S. Altmannshofer, D. Leusser and D. Stalke, *Angew. Chem. Int. Ed.*, 2011, **50**, 2845-2849; L. H. Shultz, D. J. Tempel and M. Brookhart, *J. Am. Chem. Soc*, 2001, **123**, 11539-11555; H. Xu, C. T. Hu, X. Wang and T. Diao, *Organometallics*, 2017, **36**, 4099-4102; H. Xu, P. B. White, C. Hu and T. Diao, *Angew. Chem. Int. Ed.*, 2017, **56**, 1535-1538; F. Rekhroukh, L. Estévez, C. Bijani, K. Miqueu, A. Amgoune and D. Bourissou, *Angew. Chem. Int. Ed.*, 2016, **55**, 3414-3418; R. M. Pupi, J. N. Coalter and J. L. Petersen, *J. Organomet. Chem.*, 1995, **497**, 17-25; Y. Wang, C. Qin, X.

Jia, X. Leng and Z. Huang, *Angew. Chem. Int. Ed.*, 2017, **56**, 1614-1618; A. Vigalok, O. Uzan, L. J. W. Shimon, Y. Ben-David, J. M. L. Martin and D. Milstein, *J. Am. Chem. Soc*, 1998, **120**, 12539-12544; A. Ramaraj, K. H. K. Reddy, H. Keil, R. Herbst-Irmer, D. Stalke, E. D. Jemmis and B. R. Jagirdar, *Organometallics*, 2017, **36**, 2736-2745; C. M. Klug, M. O'Hagan, R. M. Bullock, A. M. Appel and E. S. Wiedner, *Organometallics*, 2017, **36**, 2275-2284; W. H. Bernskoetter, C. K. Schauer, K. I. Goldberg and M. Brookhart, *Science*, 2009, **326**, 553-556; W. Scherer and G. S. McGrady, *Angew. Chem. Int. Ed.*, 2004, **43**, 1782-1806; C. Green Jennifer and P. Payne Martin, *Magn. Res. Chem.*, 1987, **25**, 544-549; T. S. Thakur and G. R. Desiraju, *Chem. Commun.*, 2006, 552-554; M. Etienne and A. S. Weller, *Chem. Soc. Rev.*, 2014, **43**, 242-259; B. G. Harvey and R. D. Ernst, *Eur. J. Inorg. Chem.*, 2016, 1-23; T. D. Forster, H. M. Tuononen, M. Parvez and R. Roesler, *J. Am. Chem. Soc*, 2009, **131**, 6689-6691; A. Haaland, W. Scherer, K. Ruud, G. S. McGrady, A. J. Downs and O. Swang, *J. Am. Chem. Soc,* 1998, **120**, 3762-3772; W. Scherer, D. J. Wolstenholme, V. Herz, G. Eickerling, A. Brück, P. Benndorf and P. W. Roesky, *Angew. Chem. Int. Ed.*, 2010, **49**, 2242-2246; W. Scherer, P. Sirsch, M. Grosche, M. Spiegler, S. A. Mason and M. G. Gardiner, *Chem. Commun.*, 2001, 2072-2073; W. Scherer, P. Sirsch, D. Shorokhov, G. S. McGrady, A. Mason Sax and G. Gardiner Michael, *Chem. Eur. J.*, 2002, **8**, 2324-2334; W. Scherer, V. Herz and C. Hauf, in *Electron Density and Chemical Bonding I: Experimental Charge Density Studies*, ed. D. Stalke, Springer Berlin Heidelberg, Berlin, Heidelberg, 2012, pp. 159-207; M. P. Mitoraj, A. Michalak and T. Ziegler, *Organometallics*, 2009, **28**, 3727-3733; E. Clot and O. Eisenstein, in *Principles and Applications of Density Functional Theory in Inorganic Chemistry II*, eds. N. Kaltsoyannis and J. E. McGrady, Springer Berlin Heidelberg, Berlin, Heidelberg, 2004, pp. 1-36; T. Debnath, T. Ash, T. Banu and A. K. Das, *Theor. Chem. Acc.*, 2016, **135**, 175; S. Ramakrishnan and E. D. Jemmis, *J. Organomet. Chem.*, 2018, **865**, 37-44; E.-L. Zins, B. Silvi and M. E. Alikhani, *Phys. Chem. Chem. Phys.*, 2015, **17**, 9258-9281; C. Flener-Lovitt, D. E. Woon, T. H. Dunning and G. S. Girolami, *J. Phys. Chem. A.*, 2010, **114**, 1843-1851; B. Xu, Q. Wang and X. Wang, *Comp. Theor. Chem.*, 2011, **976**, 36-41; M. Lein, *Coord. Chem. Rev.*, 2009, **253**, 625-634; W. Baratta, C. Mealli, E. Herdtweck, A. Ienco, S. A. Mason and P. Rigo, *J. Am. Chem. Soc*, 2004, **126**, 5549-5562; E. F. Van Der Eide, P. Yang and R. M. Bullock, *Angew. Chem. Int. Ed.*, 2013, **52**, 10190-10194; A. Toner, J. Matthes, S. Gründemann, H.-H. Limbach, B. Chaudret, E. Clot and S. Sabo-Etienne, *Proc. Nat. Acad. Sci. USA*, 2007, **104**, 6945-6950; S. Reinartz, P. S. White, M. Brookhart and J. L. Templeton, *J. Am. Chem. Soc*, 2001, **123**, 12724-12725; M. A. Sajjad, K. E. Christensen, N. H. Rees, P. Schwerdtfeger, J. A. Harrison and A. J. Nielson, *Chem. Commun.*, 2017, **53**, 4187-4190; M. A. Sajjad, K. E. Christensen, N. H. Rees, P. Schwerdtfeger, J. A. Harrison and A. J. Nielson, *Dalton Trans.*, 2017, **46**, 16126-16138; M. L. H. Green, *Pure Appl. Chem.*, 1984, **56**, 47-58; B. A. Arndtsen, R. G. Bergman, T. A. Mobley and T. H. Peterson, *Acc. Chem. Res.*, 1995, **28**, 154-162; L. H. Shultz and M. Brookhart, *Organometallics*, 2001, **20**, 3975-3982; R. H. Grubbs and G. W. Coates, *Acc. Chem. Res.*, 1996, **29**, 85-93; M. Hamdaoui and J.-P. Djukic, in *Noncovalent Interactions in Catalysis*, eds. K. T. Mahmudov, M. N. Kopylovich, M. F. C. Guedes.da.Silva and A. J. L. Pombeiro, The Royal Society of Chemistry, 2019, pp. 579-607.

8. M. Brookhart, M. L. H. Green and L. L. Wong, in *Carbon-Hydrogen-Transition Metal Bonds*, ed. S. J. Lippard, Wiley-Blackwell, 1988, pp. 1-124.
9. M. A. Sajjad, J. A. Harrison, A. J. Nielson and P. Schwerdtfeger, *Organometallics*, 2018, **37**, 3659-3669.
10. J. A. Harrison, A. J. Nielson, M. A. Sajjad and P. Schwerdtfeger, *Organometallics*, 2019, in press.
11. F. Weinhold, in *Encyclopedia of Computational Chemistry*, eds. P. vonRagué-Schleyer, N. L. Allinger, T. Clark, J. Gasteiger, P. A. Kollman, H. F. Schaefer and P. R. Schreiner, John Wiley & Sons, Chichester, UK, 1998, pp. 1792-1811.
12. C. Riplinger, P. Pinski, U. Becker, E. F. Valeev and F. Neese, *J. Chem. Phys.*, 2016, **144**, 024109; C. Riplinger and F. Neese, *J. Chem. Phys.*, 2013, **138**, 034106; C. Riplinger, B. Sandhoeffer, A. Hansen and F. Neese, *J. Chem. Phys.*, 2013, **139**, 134101.
13. Q. Lu, F. Neese and G. Bistoni, *Angew. Chem. Int. Ed.*, 2018, **57**, 4760-4764.
14. R. Eisenschitz and F. London, *Z. Physik*, 1930, **60**, 491-527; F. London, *Z. Phys.*, 1930, **63**, 245-279; F. London, *Trans. Faraday Soc.*, 1937, **33**, 8b-26.
15. M. J. S. Dewar, *J. Am. Chem. Soc.*, 1952, **74**, 3341-3345.
16. M. Dewar, *Bull. Soc. Chim. Fr.*, 1951, **18**, C79.
17. J. Chatt and L. A. Duncanson, *J. Chem. Soc.*, 1953, 2939-2947.
18. H. Schwarz, S. Shaik and J. Li, *J. Am. Chem. Soc.*, 2017, **139**, 17201-17212; C. Geng, J. Li, M. Schlangen, S. Shaik, X. Sun, N. Wang, T. Weiske, L. Yue, S. Zhou and H. Schwarz, *Dalton Trans.*, 2018, **47**, 15271-15277; L. Yue, N. Wang, S. Zhou, X. Sun, M. Schlangen and H. Schwarz, *Angew. Chem. Int. Ed.*, 2018, **57**, 14635-14639.
19. K. P. Wisseroth and H. Braune, *J. Phys. France*, 1977, **38**, 1249 - 1255; S. D. Deshmukh and Y. Tsori, *J. Chem. Phys.*, 2016, **144**, 191102.
20. S. Shaik, D. Danovich, W. Wu and P. C. Hiberty, *Nature Chem.*, 2009, **1**, 443.
21. G. Sini, P. Maitre, P. C. Hiberty and S. S. Shaik, *J. Mol. Struct. : THEOCHEM*, 1991, **229**, 163-188.
22. H. Hirao, H. Chen, M. A. Carvajal, Y. Wang and S. Shaik, *J. Am. Chem. Soc.*, 2008, **130**, 3319-3327.
23. A. C. Aragonès, N. L. Haworth, N. Darwish, S. Ciampi, N. J. Bloomfield, G. G. Wallace, I. Diez-Perez and M. L. Coote, *Nature*, 2016, **531**, 88; A. Masunov, J. J. Dannenberg and R. H. Contreras, *J. Phys. Chem. A*, 2001, **105**, 4737-4740; S. Sowlati-Hashjin and C. F. Matta, *J. Chem. Phys.*, 2013, **139**, 144101; F. Che, S. Ha and J.-S. McEwen, *Angew. Chem. Int. Ed.*, 2017, **56**, 3557-3561; L. Rincón, J. R. Mora, F. J. Torres and R. Almeida, *Chem. Phys.*, 2016, **477**, 1-7.
24. S. Jerhaoui, J.-P. Djukic, J. Wencel-Delord and F. Colobert, *ACS Catal.*, 2019, **9**, 2532-2542.

25. R. F. W. Bader, *Atoms in Molecules: A Quantum Theory*, Clarendon, Oxford, 1990.
26. J. Contreras-Garcia, E. R. Johnson, S. Keinan, R. Chaudret, J. P. Piquemal, D. N. Beratan and W. Yang, *J. Chem. Theor. Comp.*, 2011, **7**, 625-632; E. Johnson, S. Keinan, P. Mori-Sanchez, J. Contreras-Garcia, A. J. Cohen and W. Yang, *J. Am. Chem. Soc.*, 2010, **132**, 6498-6506.
27. M. P. Mitoraj, A. Michalak and T. Ziegler, *J. Chem. Theor. Comp.*, 2009, **5**, 962-975; M. P. Mitoraj, A. Michalak and T. Ziegler, *Organometallics*, 2009, **28**, 3727-3733.
28. T. C. Jones, A. J. Nielson and C. E. Rickard, *Aust. J. Chem.*, 1984, **37**, 2179-2192.
29. S. Grimme, A. Hansen, J. G. Brandenburg and C. Bannwarth, *Chem. Rev.*, 2016, **116**, 5105-5154.
30. M. A. Blanco, A. Martín Pendás and E. Francisco, *J. Chem. Theor. Comp.*, 2005, **1**, 1096-1109.
31. E. Francisco, A. Martín Pendás and M. A. Blanco, *J. Chem. Theor. Comp.*, 2006, **2**, 90-102; V. Tognetti and L. Joubert, *ChemPhysChem*, 2017, **18**, 2675-2687.
32. D. Suárez, N. Díaz, E. Francisco and A. Martín Pendás, *ChemPhysChem*, 2018, **19**, 973-987.
33. A. Altun, F. Neese and G. Bistoni, *J. Chem. Theor. Comp.*, 2019, **15**, 215-228.
34. S. Jerhaoui, J.-P. Djukic, J. Wencel-Delord and F. Colobert, *ACS Catalysis*, 2019.
35. Y. Dang, S. Qu, J. W. Nelson, H. D. Pham, Z.-X. Wang and X. Wang, *J. Am. Chem. Soc.*, 2015, **137**, 2006-2014.
36. A. A. Mishra, D. Subhedar and B. M. Bhanage, *Chem. Rec.*, 2018, Ahead of Print; J. Yan, Y.-B. Wang, Z.-H. Zhu, Y. Li, X. Zhu, X.-Q. Hao and M.-P. Song, *Organometallics*, 2018, **37**, 2325-2334; D. Kalyani, *Pure Appl. Chem.*, 2014, **86**, 315-319; D. Patra, P. Pattanayak, J. L. Pratihar and S. Chattopadhyay, *Polyhedron*, 2013, **51**, 46-53; J. J. Mousseau and A. B. Charette, *Acc. Chem. Res.*, 2013, **46**, 412-424; B. Vabre, F. Deschamps and D. Zargarian, *Organometallics*, 2014, **33**, 6623-6632; D. D. Beattie, A. C. Grunwald, T. Perse, L. L. Schafer and J. A. Love, *J. Am. Chem. Soc.*, 2018, **140**, 12602-12610; A. Klein, A. Sandleben and N. Vogt, *Proc. Natl. Acad. Sci., India, Sect. A*, 2016, **86**, 533-549; E. C. Volpe, A. R. Chadeayne, P. T. Wolczanski and E. B. Lobkovsky, *J. Organomet. Chem.*, 2007, **692**, 4774-4783.
37. L. S. Jongbloed, D. García-López, R. van Heck, M. A. Siegler, J. J. Carbó and J. I. van der Vlugt, *Inorg. Chem.*, 2016, **55**, 8041-8047.
38. Y.-F. Yang and Y. She, *Int. J. Quant. Chem.*, 2018, **118**, e25723.
39. M. A. Iron and T. Janes, *J. Phys. Chem. A*, 2019, **123**, 3761-3781.
40. S. Dohm, A. Hansen, M. Steinmetz, S. Grimme and M. P. Checinski, *J. Chem. Theor. Comp.*, 2018, **14**, 2596-2608.
41. D. H. Binh, M. Milovanovic, J. Puertes-Mico, M. Hamdaoui, S. D. Zaric and J.-P. Djukic, *Chem. - Eur. J.*, 2017, **23**, 17058-17069.
42. N. Agmon, *Chem. Phys. Lett.*, 1995, **244**, 456-462.
43. C. Athira and R. B. Sunoj, *Org. Biomol. Chem.*, 2017, **15**, 246-255.
44. A. V. Lee and L. L. Schafer, *Eur. J. Inorg. Chem.*, 2007, 2245 - 2255; M. B. Jones, B. S. Newell, W. A. Hoffert, K. I. Hardcastle, M. P. Shores and C. E. MacBeth, *Dalton Trans.*, 2010, **39**, 401-410.
45. G. te Velde, F. M. Bickelhaupt, E. J. Baerends, C. Fonseca Guerra, S. J. A. van Gisbergen, J. G. Snijders and T. Ziegler, *J. Comp. Chem.*, 2001, **22**, 931-967.
46. S. Grimme, J. Antony, S. Ehrlich and H. Krieg, *J. Chem. Phys.* , 2010, **132**, 154104; S. Grimme, S. Ehrlich and L. Goerigk, *J. Comp. Chem.*, 2011, **32**, 1456-1465.
47. D. G. Liakos, M. Sparta, M. K. Kesharwani, J. M. L. Martin and F. Neese, *J. Chem. Theor. Comp.*, 2015, **11**, 1525-1539; E. Paulechka and A. Kazakov, *J. Phys. Chem. A*, 2017, **121**, 4379-4387; Y. Minenkov, E. Chermak and L. Cavallo, *J. Chem. Theor. Comput.*, 2015, **11**, 4664-4676.
48. W. B. Schneider, G. Bistoni, M. Sparta, M. Saitow, C. Riplinger, A. A. Auer and F. Neese, *J. Chem. Theor. Comp.*, 2016, **12**, 4778-4792.
49. C. C. M. Samson and W. Klopper, *THEOCHEM*, 2002, **586**, 210; G. F. Mangiatordi, E. Brémond and C. Adamo, *J. Chem. Theor. Comput.*, 2012, **8**, 3082-3088.
50. V. Barone, L. Orlandini and C. Adamo, *Chem. Phys. Lett.*, 1994, **231**, 295- 300; V. Barone, L. Orlandini and C. Adamo, *Int. J. Quantum Chem.*, 1995, **56**, 697- 705; S. Sadhukhan, D. Munoz, A. Adamo and G. E. Scuseria, *Chem. Phys. Lett.*, 1999, **306**, 83- 87.
51. B. G. Johnson, C. A. Gonzales, P. M. W. Gill and J. A. Pople, *Chem. Phys. Lett.* , 1994, **221**, 100- 108; S. Patchkovskii and T. J. Ziegler, *Chem. Phys.*, 2002, **116**, 7806- 7813.
52. D. L. Davies, S. M. A. Donald, O. Al-Duaij, S. A. Macgregor and M. Poelleth, *J. Am. Chem. Soc.*, 2006, **128**, 4210-4211.
53. J. P. Perdew, K. Burke and M. Ernzerhof, *Phys. Rev. Lett.*, 1996, **77**, 3865-3868.
54. E. van Lenthe, E. J. Baerends and J. G. Snijders, *J. Chem. Phys.*, 1993, **99**, 4597-4610; E. van Lenthe, E. J. Baerends and J. G. Snijders, *J. Chem. Phys.*, 1994, **101**, 9783-9792; E. van Lenthe, A. Ehlers and E.-J. Baerends, *J. Chem. Phys.*, 1999, **110**, 8943-8953.
55. F. Neese, *WIREs Compt. Mol. Sci.*, 2012, **2**, 73-78.
56. F. Weigend and R. Ahlrichs, *Phys. Chem. Chem. Phys.*, 2005, **7**, 3297-3305.
57. G. L. Stoychev, A. A. Auer and F. Neese, *J. Chem. Theor Comp.*, 2017, **13**, 554-562.

Table of Content Graphic.